Colorization of Fusion Image of Infrared and Visible Images Based on Parallel GANs

LEI CHEN[1], JUN HAN[1], FENG TIAN[2]

1Xi'an Technological University, Xi'an, Shaanxi Province, 710021, China

2Bournemouth University, Poole, BH12 5BB, UK

Abstract: Fusing the infrared and visible images has many advantages and can be applied to applications such as target detection and recognition. Colors can give more accurate and distinct features, but the low resolution and low contrast of fused images make this a challenge task. In this paper we proposed a method based on parallel GANs to address the challenge. We considered infrared image, visible image and fusion image as chroma and luminance of the Lab color model. Then we constructed three parallel GANs to generate luminance and chroma data of the Lab model. The Lab data were then converted to RGB image. Experiment results have demonstrated that the proposed approach is able to achieve better performance against existing methods.

1、Introduction

In recent years, the infrared and visible image fusion technology has been widely used in target detection and recognition. Especially under the low-light and obstacles obstruction, the fusion image combines the advantages of the two kinds of images, which can not only detect the hidden target, but also provide rich detailed information [1~6]. Color information can improve the visual perception and make the area and target of the scene clearer, but there is no color information in the IR image and visible image in low light condition such as Fig. 1. Therefore, the color restoration of fusion image is very important for scene recognition and target detection under that condition.

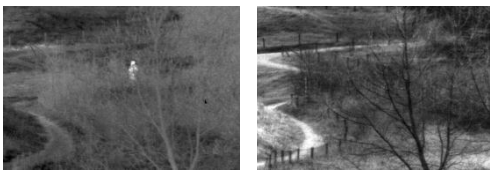

Fig.1. IR image and low-light image

For the fusion of IR image and visible image, many scholars have proposed many excellent methods which based on deep learning (DL). Xu, et.al. [7] proposed a new unsupervised and unified densely connected network for different types of image fusion under elastic weight consolidation. Xu, et.al [8] proposed a unified and unsupervised end-to-end network to address different fusion problems. Ma, et.al. [9] proposed dual-discriminator conditional generative adversarial network to fuse infrared and visible images of different resolutions. Ma, et.al. [10] proposed an end-to-end model for infrared and visible image fusion based on detail preserving adversarial learning. Ma, et.al. [11] presented a novel IR and visible image fusion algorithm, FusionGAN, based on a generative adversarial network (GAN). Through comparison and analysis of the approaches mentioned above, in this paper we have selected the fusion results of FusionGAN as our target to color.

The result of color restoration of gray-scale images could be ambiguous as there may be a variety of color attributes for a gray-scale object. Nevertheless, many approaches have been proposed over the past decade [12~17].The fusion image of infrared and visible is very different from the gray-scale image, having low resolution and contrast. Moreover, only the chroma of the image needs to be considered for gray-scale image colorization. For fusion image, not only the chroma but also the luminance of the image should be considered in the process of colorization. More importantly, the colorization of gray-scale images have ground-truth image in the training process, while the IR and low-light images obtained under low-light conditions don't

have color images. All these factors render the difficulty of colorization of the fusion image.

Recently, convolutional neural network (CNN) has set off a wave of research in the field of image. Inspired by GAN, we designed parallel GANs based on the Lab color model to color the fusion image. We assign the infrared, low-light-level and fusion images to the Lab model reasonably, which sets up luminance reference and chromaticity reference of GAN model, and achieves good coloring effect by designing reasonable anti-loss function.

Among the remaining sections of this paper, Section 2 reviews traditional and DL-based colorization methods. Section 3 presents the proposed method, including the network structure and loss function. Section 4 gives our experimental results, including qualitative illustration and quantitative analysis and comparison to the state-of-arts. Section 5 concludes the paper with future work.

2、Related work

In recent years, many researchers have proposed many gray-scale image coloring methods, which can be divided into two categories: one is traditional method, and the other is DL-based method. The tradition method needs human intervention and guidance to generate the image's color. It includes some approaches such as the manual selection of area color [18], the labeling of the image [19], the extraction of image features to generate semantic images [20], and the assignment of similar scene color image as reference to realize color coloring [21~23]. These methods can achieve gray-scale image coloring to some extent, but they have some limitations. They not only need human intervention, but also require the basic color information of each area or the understanding of the semantic and scene information of the image. Moreover, there is no way to achieve end-to-end automatic coloring.

With the increasingly extensive application of DL, many scholars have proposed CNN-based coloring algorithms. Cheng, et.al. used patch technology to automatically color images with similar patches in vast of color image data sets [24]. However, this method needs a large number of color image data sets, and can only achieve a certain extent when there are no similar patches in the data set. Ye, et.al. proposed a mixed image coloring method which contains two modules [25]. First, it used the Mask R-CNN model to segment the image, and then match reference color image. Second, it used U-Net model and VGG model to color each region. Finally, it used Poisson technology to fuse all the color images to get the final image. G, et.al. proposed an approach to leverage recent advances in deep networks, exploiting both low-level and semantic representations during colorization [26]. S et.al. proposed to integrate local small image information based on CNN to calculate the global priors, and then train the model by using the large-scale scene data set after the label operation [27]. The category label can be used to learn the global priors effectively and discriminatively. R, et.al. proposed to use many color data sets to train the feed forward CNN [28], and finally decompose the color image into the Lab color image model to generate color.

There are many other CNN-based gray-scale image coloring methods. Larsson, et.al. proposed that color images could be generated automatically by using a trained model to predict the per-pixel color histogram [26]. Su, et.al. proposed two neural networks which were used to gain the components of U and V in the YUV color model [29], and then two losses were used to suppress errors in the training. These methods have achieved some success, but they need a large number of data sets to train the model while building the model and network.

With the rise of the GAN, researchers have introduced it into the field of image coloring. Kamyar, et.al. proposed to use Conditional Deep Convolution Generated Adversarial Network (DCGAN) to color gray-scale images [30]. Patricia, et.al proposed to use semantic

information to infer the color information [31]. Quentin, et.al. proposed to use DRANGAN to achieve the color mapping of gray-scale aerial photos [32]. Mohammad, et.al. proposed to use parallel loops to generate a consistent confrontation network, and use color images with similar context to train the network, and finally use it to generate image color. Raggi, et.al. proposed to use capsule network instead of CNN in GAN to color gray image [33].

The methods above mainly target images with high resolution. Recently, some scholars have also proposed coloring methods for low-resolution images. For example, Gu, et.al. proposed an algorithm for coloring thermal radiation images [34]. First, the thermal radiation images are segmented and each area is classified and labeled, then Markov decision process is introduced to deal with color estimation. Kuang, et.al. adds compound loss based on traditional GAN [35], which includes content, antagonism, perception and total variation loss for processing infrared image colorization. But these methods need the ground truth for training.

Our goal is to color the fusion image with low resolution and low contrast without the need of ground truth. We aim to get the colorful image which rich in color and distinct regional color differences. Therefore, this paper proposes to construct Lab color model using infrared, visible and fusion images, and then construct parallel GANs model to conduct adversarial training for luminance and chromaticity respectively.

3、Proposed method

Lab color model composed of three elements, one element is luminance (L), and ‘a’ and ‘b’ are two color channels. The ‘a’ channel represents the color range from dark green to gray to bright pink. The ‘b’ channel represents the color range from bright blue to gray to yellow. The Lab model has wide color gamut, and can expressed all colors that human eyes may perceive. The fusion image combines the advantages of infrared and visible light, and can reflect the luminance of the whole scene, so it can use as the reference of L. The infrared image is the thermal radiation information of various substances in the scene, which can reflect the information of channel ‘a’, while visible light can add the information of channel ‘b’ in the Lab model. Inspired by Lab color model and GAN, we designed ‘a’ parallel GANs algorithm for complex luminance and chromaticity on the basis of existing fused images.

3.1. The structure of the parallel GANs

Our GAN model has three parallel GANs that have the similar structure as shown below in Fig. 2.

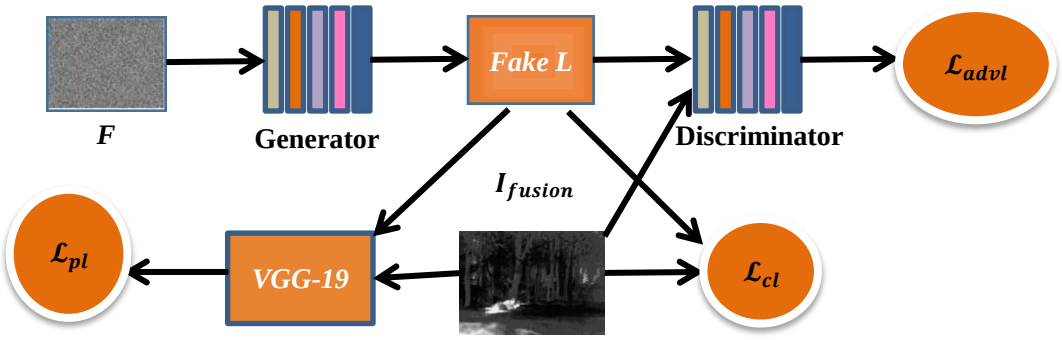

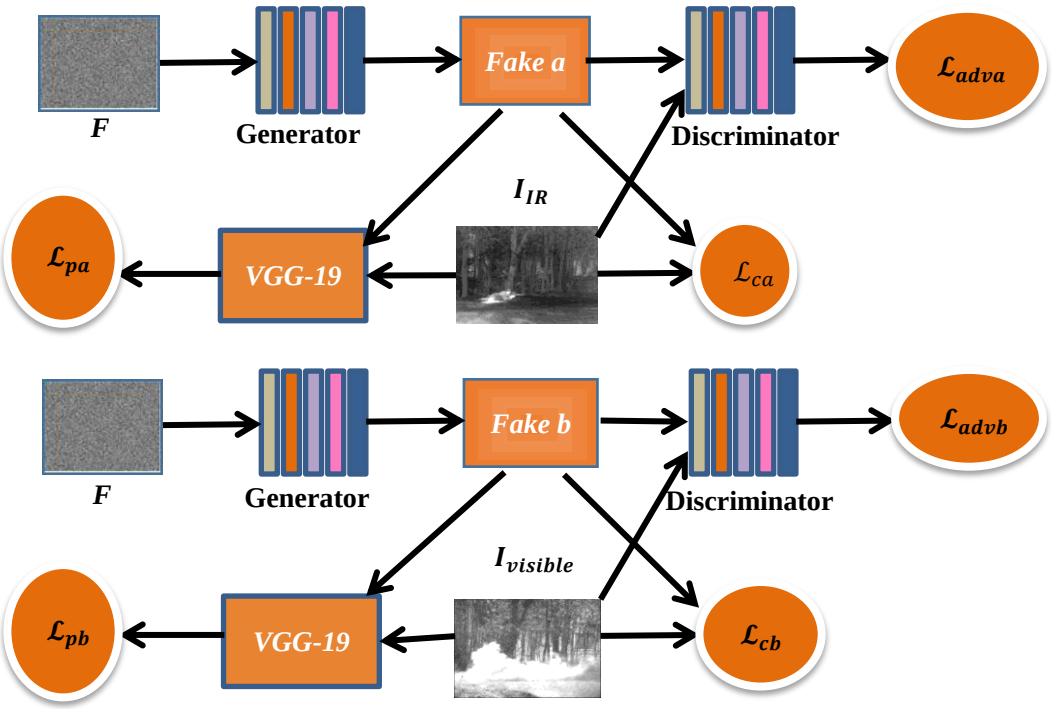

Fig. 2. The framework of the parallel GANs

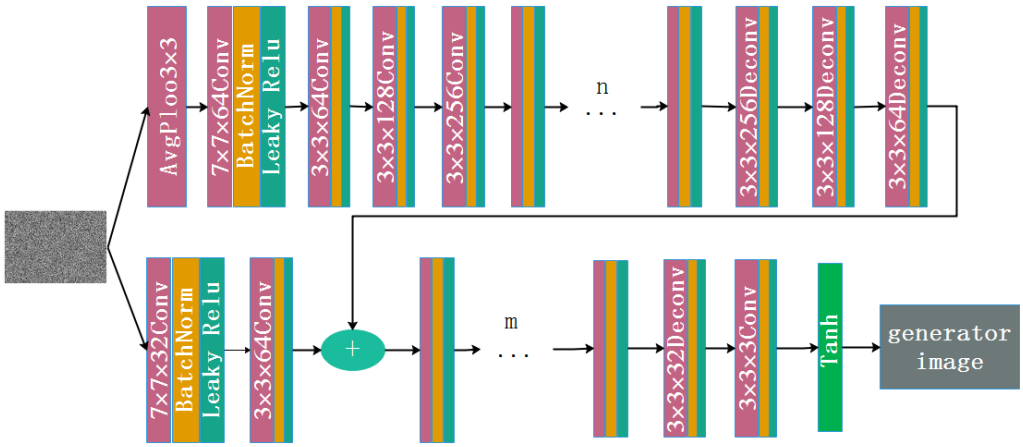

Fig. 3. The structure of the generator

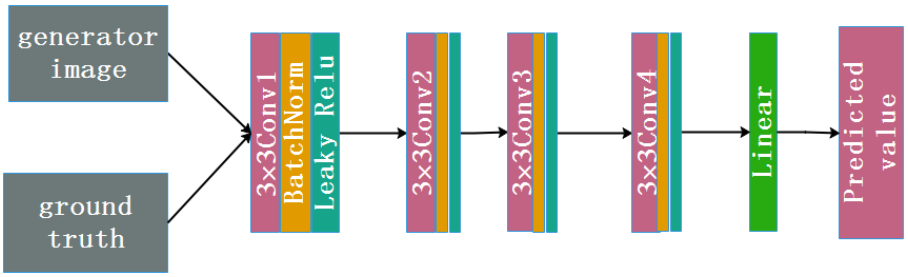

Fig. 4. The network structure of the discriminator

The first GAN is to generate the luminance data using the fused image as the ground truth. The second and third are to generate the chroma data in the Lab model using IR and low-light images as the ground truth respectively. After the three parallel GANs training, our network can generate the luminance and chroma data at the same time. Finally, the Lab model is converted to RGB format image.

Our model has three generators that have

the same structure as shown in Fig. 3. The structure follows the one proposed by Johnson [36]. Our model has three discriminators that have the same structure as shown in Fig. 4.

The discriminator is a simple five-layer CNN, the first four layers have 3×3 filters. The stride in each layer set as 2, and there is no padding during convolution operation. This is different from the generator, for the D is using feature map extracts from the source image to identify whether is true or false. We do not pad the input image for avoiding introduces noise.

3.2. The Loss Function

Based on the traditional GAN loss function, we introduce the perceptual loss, which can increase the detail of the generated image. So our loss function contains three losses which include content, adversarial and perceptual losses.

Content loss:

$$\mathcal{L}_{\mathrm{ca}} = \mathbb{E}_{\mathrm{a}\sim \mathrm{I_{IR}}}[||\mathrm{G}(\mathrm{F_z}) - \mathrm{I_{IR}}||_2^2] \quad (1)$$

$$\mathcal{L}_{\mathrm{cb}} = \mathbb{E}_{\mathrm{b}\sim \mathrm{I_{visible}}}[||\mathrm{G}(\mathrm{F_z}) - \mathrm{I_{visible}}||_2^2] (2)$$

$$\mathcal{L}_{\mathrm{cl}} = \mathbb{E}_{\mathrm{l}\sim \mathrm{I_{fusion}}}[||\mathrm{G}(\mathrm{F_z}) - \mathrm{I_{fusion}}||_2^2] \quad (3)$$

Where $\mathcal{L}_{\mathrm{ca}}$ represents the content loss of channel a in LAB color model, $\mathcal{L}_{\mathrm{cb}}$ represents the content loss of channel b in LAB color model, $\mathcal{L}_{\mathrm{cl}}$ represents the content loss of channel L in LAB color model. $\mathrm{I_{IR,}}\mathrm{I_{visible}}$ and $\mathrm{I_{fusion}}$ denotes the infrared image, visible light image and fusion image respectively. $||\cdot||_2$ denotes the Euclidean norm.

Adversarial loss:

$$\mathcal{L}_{\mathrm{adva}} = \mathbb{E}_{\mathrm{a}}[-\log(\mathrm{D}(\mathrm{G}(\mathrm{F_z})) - \mathrm{I_{IR}}] \quad (4)$$

$$\mathcal{L}_{\mathrm{advb}} = \mathbb{E}_{\mathrm{b}}[-\log(\mathrm{D}(\mathrm{G}(\mathrm{F_z})) - \mathrm{I_{visible}}] (5)$$

$$\mathcal{L}_{\mathrm{advl}} = \mathbb{E}_{\mathrm{l}}[-\log(\mathrm{D}(\mathrm{G}(\mathrm{F_z})) - \mathrm{I_{fusion}}] (6)$$

Where $\mathcal{L}_{\mathrm{adva}}$ represents the adversarial loss of a channel, $\mathcal{L}_{\mathrm{advb}}$ represents the adversarial loss of b channel, $\mathcal{L}_{\mathrm{advl}}$ represents the adversarial loss of L channel. $\mathrm{F_z}$ denotes the input noise image.

Perceptual loss:

Adversarial loss is easy to produce deformed texture in our work. To mitigate the modification problem, we used the ReLU function of VGG-19 in [37] to activate the perceptual loss, which is beneficial for the texture to remain in the high level space.

$$\mathcal{L}_p = \frac{1}{s_k}\sum_{m=1}^{n}\frac{1}{H_k W_k}\sum_{i=1}^{H_k}\sum_{j=1}^{W_k}||\psi_k(y_{i,j})_m - \psi_k(G(x_{i,j}))_m||_1 \quad (7)$$

Where $\psi_k(\cdot)$ represents feature representation of the KTH maxpooling layer in VGG-19, H_k and W_k represents the length and width of the feature image, $\mathrm{s_k}$ represents the number of feature images.

Total loss:

$$\mathcal{L}_t = \lambda_c\mathcal{L}_c + \lambda_a\mathcal{L}_a + \lambda_p\mathcal{L}_p \quad (8)$$

In the formula, $\mathcal{L}_{\mathrm{c}}$ represents one of the content losses, i.e., $\mathcal{L}_{\mathrm{ca}}$、$\mathcal{L}_{\mathrm{cb}}$ or $\mathcal{L}_{\mathrm{cl}}$. $\mathcal{L}_{\mathrm{a}}$ represents one of the adversarial losses, i.e., $\mathcal{L}_{\mathrm{adva}}$、$\mathcal{L}_{\mathrm{advb}}$ or $\mathcal{L}_{\mathrm{advl}}$. λ_{c}、λ_{a} and λ_{p} are weight coefficients of content loss, adversarial loss and perceptual loss respectively, which are used to control the share of each loss function in the overall loss function.

4、Experiment

To evaluate our method, we use TNO dataset [38] and RoadScene dataset [8]. We gain three images per group: visible image, infrared image and fusion image in low light. Then we divided them into two groups, one containing 33 images for training the network, and the other containing 8 images for testing. The training network data of 33 groups of images is not enough, so we clipped the images of each group into 120×120 image blocks and moved at a pace of 12. In this way, we gained 44,691 training image patches, which ensured the adequacy of training data.

In the first layer convolution between the generator and the discriminator in our GAN structure, total 32 layers are used. The parameters m and n in the Generator are set to 3 and 9, respectively. The weight coefficients λ_{c}、λ_{a} and

λ_p are set to 1, 0.06 and 1, respectively. We calculate the perceptual losses ψ_6、ψ_{11}、ψ_{17} and ψ_{23}. During the process we use the method [39] to optimize the discriminator.

To elaborate and compare the effects clearly, we obtained the colorization results by 3 different methods of 8 pairs as show in Fig. 5 and Fig. 6. The comparing methods in our experiment include Larsson G's method [26], Iizuka S' method [27] and Zhang R's method [28]. We obtained the results from the net..

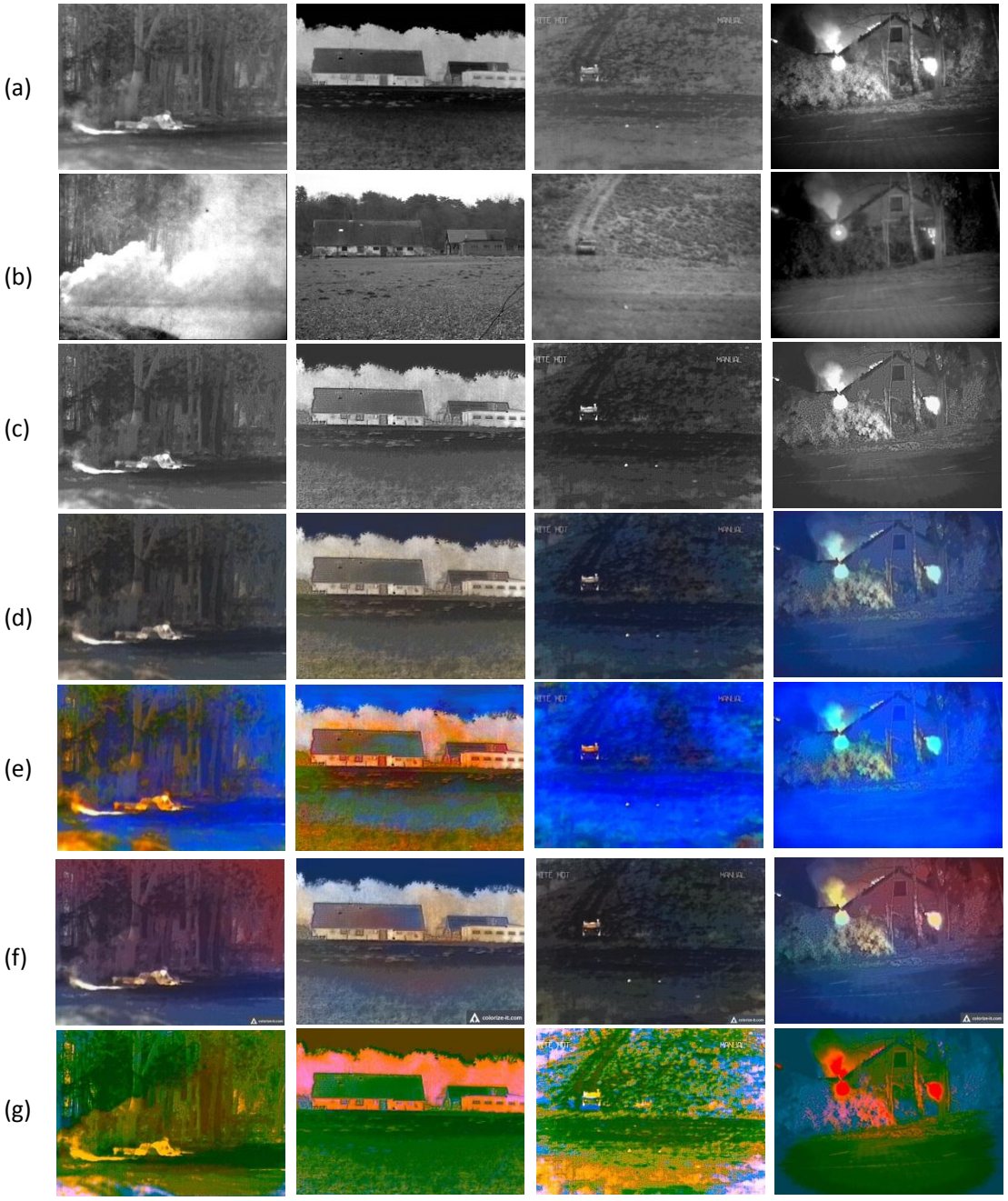

Fig.5. The coloring results for TNO dataset. (a) IR image, (b) visible image, (c) fused image,

(d) from Iizuka S' method, (e) from Larsson G's method (f) from Zhang R's method, (g) from OURS

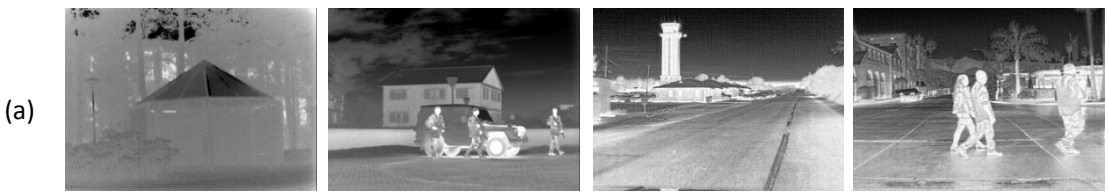

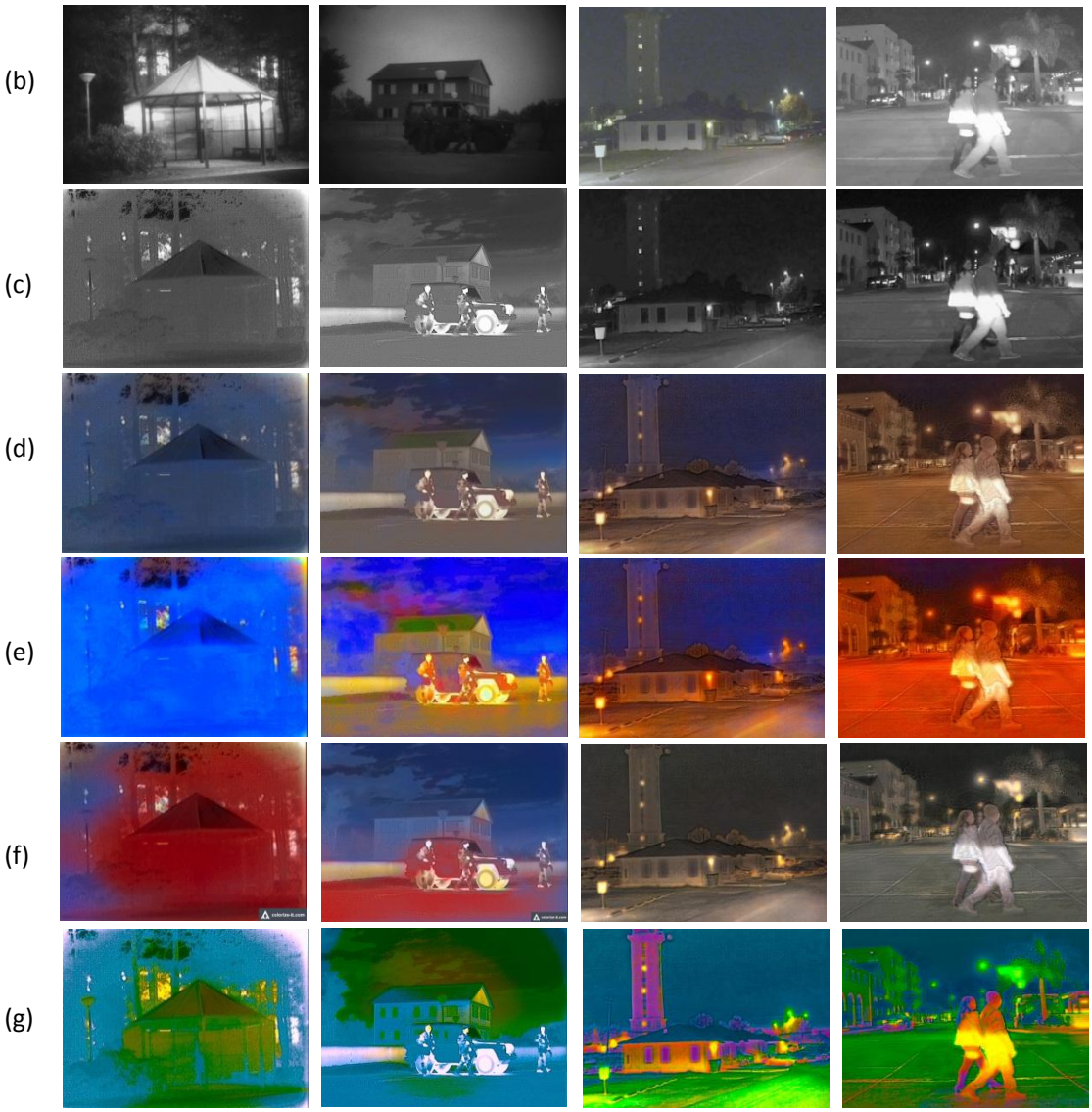

Fig. 6. The coloring results for RoadScene dataset. (a) IR image, (b) visible image, (c)fusion image, (d) from Iizuka S' method, (e) from Larsson G's method (f) from Zhang R's method, (g) from OURS

4.1. Qualitative evaluation

From the experimental results, we can see Iizuka S' method not well realize the generation of color, as the images in column 1 and 2 of d in Fig. 5 and column 2 of d in Fig. 6 show basically no color change between the coloring results and the fused image. The images in column 3 and 4 of d in Fig. 5 only show some light blue color. The images in column 3 and 4 of d in Fig. 6 show certain color but it's a long way from being colorful. Only the image of column 2 of d in Fig. 6 of each region implements a simple color to distinguish, but not quite clear.

Compared with Iizuka S' method, Larsson G's method generates better color. The images in column 3 and 4 of e in Fig. 5 and column 1 of e in Fig. 6 blue fill the entire picture, color distinctions are not implemented. The images in column 1 and 2 of e in Fig. 5 and column 2 of e in Fig. 6 only generate some rich color, but the background color of the whole image is fuzzy chaos. The colors of the images in column 3 and 4 of e in Fig. 6 are basically the same, without a good regional color distinction.

Zhang R's method achieves better results than Larsson G's method and Iizuka S' method. The color in the image does not reflect the regional differences, and there is no significant

change of color at the edges of the region. The coloring results still look unrealistic. The houses, trees, cars and smoke in the pictures are very fuzzy, lacking fine texture. The main reason is that the fusion image combines the characteristics of low-light-level and IR, which leads to low contrast and low resolution. So using high resolution and high contrast color image is not effective on training network for the fusion image.

Our method is superior to the other methods and achieves the coloring results that reflect the information of low-light and IR. Different areas in the image are clearly segmented by different colors. In the image of column 1 of g in Fig. 5, the three parts of the forest, the soldier and the smoke are clearly differentiated by different colors. The area covered by smoke and the jungle that is not covered in the image of column 3 of g in Fig. 5 are distinguished by dark green, light green and yellow, respectively. The representation of the light in column 4 of g in Fig. 5 is particularly accurate, represented in red, which reflects the high heat of the IR and the distinction between the range of heat coverage and that of no heat coverage. In the image of column 2 of g in Fig. 6 is there a part of the dark green range that is very abrupt. In fact, this is the reflection of the part of the low-light image where the luminance is particularly prominent. Overall, the generated color realizes the distinction of different regions, with the IR and low light information clearly reflected in the color image. There is no blurring in the image, and the fine texture information is also clearly reflected.

4.2. Quantitative evaluation

It is difficult to evaluate the coloring quality of fused images, especially when there is no ground truth for reference in our task. In this paper we select the peak signal-to-noise ratio (PSNR) [40] and Color saturation (CS) to objectively evaluates the richness in color and the distinct regional color differences, as shown in Table 1.

Table 1. The average values of two data set

Methods	TNO		RoadScene	
	PSNR	CS	PSNR	CS
Iizuka S’	10.23	0.26	13.43	0.62
Larsson G’s	13.48	0.47	15.8	0.74
Zhang R’s	15.78	0.58	12.38	0.58
OURS	**21.56**	**0.78**	**20.89**	**0.84**

Clearly it can be seen that our method outperforms Larsson G’s method, Iizuka S' method and Zhang R’s on both criteria. This shows that our method performs well in terms of global quality and local perception as well as chromaticity.

5、Conclusion

In this paper, we propose a parallel GANs approach to color the fusion images of infrared image and low light level image. Making full use of the information from three images, we apply the complex loss of content, confrontation and perception to realize the simultaneous generation of Lab channels in GAN network. Quantitative and qualitative evaluations from experiments show that our method is superior to the most advanced deep learning-based methods [26~28]. In the future we will study new approaches to add semantic information into the fusion color generation, thus achieving more accurate color.

Acknowledgments

This work was supported by the National Natural Science Foundation of China under Grant 61572392 and by the National and Local Funds for New Networks and Measurement and Control Laboratories under Grant GSYSJ2017001.

Disclosures statement

The authors declare that there are no conflicts of interest.

References

[1] Cheng Zhao, Yongdong Huang, Shi Qiu. Infrared and image fusion algorithm based on saliency detection and adaptive double-channel spiking

cortical model. Infrared Physics & Technology, 2019.
[2] Xin Jin, Qian Jiang, Shaowen Yao,et al. Infrared and visual image fusion method based on discrete cosine transform and local spatial frequency in discrete stationary wavelet transform domain. Infrared Physics & Technology,2018,88
[3] Yunfan Chen and Hyunchul Shin. "Multispectral image fusion based pedestrian detection using a multilayer fused deconvolutional single-shot detector." JOSA A 37, no. 5 (2020): 768-779.
[4] Ruichao Hou, Dongming Zhou, Rencan Nie, Dong Liu, Lei Xiong, Yanbu Guo, and Chuanbo Yu. "VIF-Net: an unsupervised framework for infrared and visible image fusion." IEEE Transactions on Computational Imaging 6 (2020): 640-651.
[5] Jiangtao Xu, Xingping Shi, Shuzhen Qin, Kaige Lu, Han Wang, and Jianguo Ma. "LBP-BEGAN: A generative adversarial network architecture for infrared and visible image fusion." Infrared Physics & Technology 104 (2020): 103144.
[6] Qilei Li, Lu Lu, Zhen Li, Wei Wu, Zheng Liu, Gwanggil Jeon, and Xiaomin Yang. "Coupled GAN with relativistic discriminators for infrared and visible images fusion." IEEE Sensors Journal (2019).
[7] Xu H , Ma J , Le Z , et al. FusionDN: A Unified Densely Connected Network for Image Fusion[J]. Proceedings of the AAAI Conference on Artificial Intelligence, 2020, 34(7):12484-12491.
[8] Xu H , Ma J , Le Z , et al. U2Fusion: A Unified Unsupervised Image Fusion Network[J]. TPAMI.2020. 3012548
[9] Ma J, Xu H, Jiang JJ, et al.DDcGAN: A Dual-discriminator Conditional Generative Adversarial Network for Multi-resolution Image Fusion, IEEE TIP, 2020.29.4980-4995
[10] A J M , A P L , A W Y , et al. Infrared and visible image fusion via detail preserving adversarial learning[J]. Information Fusion, 2020, 54:85-98.
[11] Ma J , Yu W , Liang P , et al. FusionGAN: A generative adversarial network for infrared and visible image fusion[J]. Information Fusion, 2019, 48:11-26.
[12] Zhengmeng Jin, Chen Zhou. A Coupled Total Variation Model with Curvature Driven for Image Colorizarion [J]. Inverse Problems and Imaging. Volume 10, No. 4, 2016, 1037–1055
[13] Zezhou Cheng, Qingxiong Yang, Bin Sheng. IEEE Transactions on Image Processing. VOL. 26, NO. 11, November 2017
[14] Hu M , Ou B , Xiao Y . Efficient image colorization based on seed pixel selection[J]. Multimedia Tools and Applications, 2017, 76(22):23567-23588.
[15] Li F , Ng M K . Image colorization by using graph bi-Laplacian[J]. Advances in Computational Mathematics, 2019.
[16] Mamoru Sugawara, Kazunori Uruma, Seiichiro Hangai, Takayuki Hamamoto. Local and Global Graph Approaches to Image Colorization[J]. IEEE SIGNAL PROCESSING LETTERS, VOL. 27, 2020
[17] Jiancheng An,Koffi Gagnon Kpeyiton,Qingnan Shi,Grayscale images colorization with convolutional neural networks[J]. Soft Computing,https://doi.org/10.1007/s00500-020-04711-3
[18] A. Levin, D. Lischinski, Y. Weiss, Colorization using optimization[C]//ACM transactions on graphics (tog), ACM 23 (3) (2004) 689–694.
[19] Q. Luan, F. Wen, D. Cohen-Or, et al., Natural image colorization[C], Proceedings of the 18th Eurographics conference on Rendering Techniques. Eurographics Association, 2007, pp. 309–320.
[20] Zhao J , Han J , Shao L , et al. Pixelated Semantic Colorization[J]. International Journal of Computer Vision, 2019(1).
[21] Li B , Zhao F , Su Z , et al. Example-Based Image Colorization Using Locality Consistent Sparse Representation[J]. IEEE Transactions on Image Processing, 2017, PP(99):1-1.
[22] Li B , Lai Y K , Rosin P L . Example-based Image Colorization via Automatic Feature Selection and Fusion[J]. Neurocomputing, 2017, 266:687-698.
[23] T. Welsh, M. Ashikhmin, K. Mueller, Transferring color to greyscale images[C],ACM Trans. Graph. (TOG) ACM 21 (3) (2002) 277–280.
[24] Cheng Z , Yang Q , Sheng B . Deep Colorization[C]// 2015 IEEE International Conference on Computer Vision (ICCV). IEEE, 2015.
[25] Ye W , Chen H , Zhang Z , et al. Hybrid Scheme of Image's Regional Colorization Using Mask R-CNN and Poisson Editing[J]. IEEE Access, 2019, PP(99):1-1.
[26] Larsson G , Maire M , Shakhnarovich G . Learning Representations for Automatic Colorization[C]// European Conference on Computer Vision. Springer International Publishing, 2016.
[27] Iizuka S , Simo-Serra E , Ishikawa H . Let there be color!: joint end-to-end learning of global and local image priors for automatic image colorization with simultaneous classification[J]. ACM Transactions on Graphics, 2016, 35(4):110.1-110.11.
[28] Zhang R , Isola P , Efros A A . Colorful Image Colorization[J]. 2016.
[29] A Z S , A X L , A J G , et al. An edge-refined vectorized deep colorization model for grayscale-to-color images[J]. Neurocomputing, 2018, 311:305-315.
[30] Nazeri K , Ng E , Ebrahimi M . Image Colorization Using Generative Adversarial Networks[M]// Articulated Motion and Deformable Objects. Springer, Cham, 2018.
[31] Vitoria P , Cisa L R , Ballester C . ChromaGAN: Adversarial Picture Colorization with Semantic Class Distribution[C]// IEEE Winter Conference on Applications of Computer Vision. IEEE, 2020.
[32] Poterek Q , Herrault P A , Skupinski G , et al. Deep Learning for Automatic Colorization of Legacy Grayscale Aerial Photographs[J]. IEEE Journal of Selected Topics in Applied Earth Observations and Remote Sensing, 2020, PP(99):1-1.
[33] Johari M M , Behroozi H . Context-Aware Colorization of Gray-Scale Images Utilizing a Cycle-Consistent Generative Adversarial Network Architecture[J]. Neurocomputing, 2020, 407.

[34] Xiaojing Gu, Mengchi He, Xingsheng Gu. Thermal image colorization using Markov decision processes[J]. Memetic Computing, 2017.
[35] X Kuang，X Sui，C Liu，L Yuan，G Gu. Thermal Infrared Colorization via Conditional Generative Adversarial Network[J]. Infrared Physics & Technology,107(2020) 103338
[36] J. Johnson, A. Alahi, L. Fei-Fei, Perceptual losses for real-time style transfer and super-resolution[C]//European Conference on Computer Vision, Springer, Cham, 2016, pp. 694–711.
[37] J. Johnson, A. Alahi, L. Fei-Fei, Perceptual losses for real-time style transfer and super-resolution[C]//European Conference on Computer Vision, Springer, Cham,2016, pp. 694–711.
[38] A. Toet, E.M. Franken, Perceptual evaluation of different image fusion schemes, Displays 24 (1) (2003) 25–37 https://figshare. com/articles/ TNO_Image_Fusion_Dataset/ 1008029.
[39] S. Hwang, J. Park, N. Kim, et al., Multispectral pedestrian detection: Benchmark dataset and baseline[C], Proceedings of the IEEE Conference on Computer Vision and Pattern Recognition, 2015, pp. 1037–1045.
[40] N. Damera-Venkata, T.D. Kite, W.S. Geisler, et al., Image quality assessment based on a degradation model, IEEE Trans. Image Process. 9 (4) (2000) 636–650.